Journal of Dental Research
2018, Vol. 97(12) 1383–1390

DOI: 10.1177/0022034518777751
journals.sagepub.com/home/jdr

The Zonal Architecture of the Mandibular Condyle Requires ADAMTS5

A.W. Rogers[1], S.E. Cisewski[1], and C.B. Kern[1]

Abstract

Temporomandibular joint (TMJ) osteoarthritis (TMJOA) disrupts extracellular matrix (ECM) homeostasis, leading to cartilage degradation. Upregulated a disintegrin and metalloproteinase with thrombospondin motifs (ADAMTS)–5 leads to cleavage of its substrate aggrecan (Acan) and is considered a hallmark of TMJOA. However, most research on ADAMTS5-Acan turnover has focused on hyaline cartilage, not fibrocartilage, which comprises the TMJ. The mandibular condylar cartilage (MCC) of the TMJ is organized in zones, and chondrocytes are arranged in axial rows, yet the molecular mechanisms required to generate the MCC zonal architecture have not been elucidated. Here, we test the hypothesis that ADAMTS5 is required for development of the TMJ MCC. *Adamts5*$^{+/+}$ and *Adamts5*$^{-/-}$ murine TMJs were harvested at postnatal day 7 (P7), P21, 2 mo, and 6 mo of age; histomorphometrics indicated increased ECM. Immunohistochemistry and Western blots demonstrated the expanded ECM correlated with increased Acan localization in *Adamts5*$^{-/-}$ compared to *Adamts5*$^{+/+}$. Cell volume was also decreased in the MCC of *Adamts5*$^{-/-}$ due to both a reduction in cell size and less mature hypertrophic chondrocytes. Analysis of chondrogenic maturation markers by quantitative real-time polymerase chain reaction indicated *Col2a1*, *Col10a1,* and *Sox9* were significantly reduced in *Adamts5*$^{-/-}$ MCC compared to that of *Adamts5*$^{+/+}$. The older (6 mo) *Adamts5*$^{-/-}$ MCC exhibited changes in chondrogenic cell arrangements, including clustering and chondrogenic atrophy, that correlated with early stages of TMJOA using modified Mankin scoring. These data indicate a potentially novel and critical role of ADAMTS5 for maturation of hypertrophic chondrocytes and establishment of the zonal architecture that, when disrupted, may lead to early onset of TMJOA.

Keywords: cell differentiation, cell-matrix interactions, temporomandibular disorders (TMDs), matrix biology, matrix metalloproteinases (MMPs), extracellular matrix

Introduction

The temporomandibular joint (TMJ) is a load-bearing structure that facilitates mandibular movements. Fibrocartilage covers the bony surfaces of the mandibular condyle and glenoid fossa and is unique compared to other joints such as the knee and hip, which are composed of hyaline cartilage (Benjamin and Ralphs 2004). Cells located in the fibrocartilage of the mandibular condyle, also referred to as the mandibular condylar cartilage (MCC), are organized into zones and arranged in axial rows. Each zone represents a different maturational stage designated as superficial, polymorphic, chondrocytic, and hypertrophic (Chen et al. 2012). Biomechanical forces generated by use of the joint initiate signaling cascades, which promote chondrocyte maturation (Rabie et al. 2004; Sobue et al. 2011). Although the basic zonal organization of fibrocartilage is known, the molecular mechanisms involved remain poorly understood.

The MCC is avascular, requiring cells in each zone to communicate and survive in their unique and complex extracellular matrix (ECM). The ECM is rich in hyaluronan, collagens, and proteoglycans, which generate a scaffold that stores growth factors and various signaling ligands (Gao et al. 2014). The ECM also gives cartilage its compressibility and structure to withstand loading on the joint. It is subdivided into the interterritorial matrix (ITM) and the pericellular matrix (PCM). The PCM is a thin region of specialized ECM that directly surrounds chondroprogenitors and chondrocytes. Given the proximity of the PCM to the cell, it plays a role in influencing cell identity, behavior, and homeostasis via the mechanotransduction of appropriate maturation signals (Chu et al. 2017; Wilusz et al. 2014). Aggrecan (Acan), the most abundant proteoglycan in the cartilage, is localized to the PCM of articular chondrocytes in hyaline cartilage and interacts with CD44-bound hyaluronan; however, the PCM of the chondrocytic and hypertrophic cells in the TMJ has not been elucidated (Embree et al. 2010; Knudson 1993). Acan is cleaved in a stepwise manner by ECM proteases, including a disintegrin and metalloproteinase with thrombospondin motifs (ADAMTSs) and matrix metalloproteinases (MMPs), to produce aggrecan fragments with neoepitopes (Fosang et al. 2010). This process is upregulated in TMJ osteoarthritis (TMJOA), where Acan is the first ECM

[1]Department of Regenerative Medicine and Cell Biology, Medical University of South Carolina, Charleston, SC, USA

A supplemental appendix to this article is available online.

Corresponding Author:
C.B. Kern, Department of Regenerative Medicine and Cell Biology, Medical University of South Carolina, 171 Ashley Avenue, Charleston, SC 29425, USA.
Email: kernc@musc.edu

component to be degraded (Pratta et al. 2003). Late-stage TMJOA is characterized by cartilage degradation due to a disruption in Acan homeostasis via ADAMTSs and MMPs (Embree et al. 2010).

ADAMTS5, a member of the subfamily of aggrecanases (Kintakas and McCulloch 2011; Kelwick et al. 2015), exhibits the most efficient proteolytic activity against Acan and is the major cartilage protease (Stanton et al. 2005). Studies have demonstrated that ADAMTS5 is upregulated in osteoarthritis (OA) of both the knee and TMJ, emphasizing ADAMTS5's deleterious role (Plaas et al. 2007; Kintakas and McCulloch 2011; Li et al. 2014). In fact, ADAMTS5 deletion was shown to be protective against cartilage degradation in a knee OA model. However, ADAMTS5 deficiency has not been evaluated in fibrocartilage during development, homeostasis, or disease (Glasson et al. 2005). Other studies emphasize the importance of ADAMTS5 during development; ADAMTS5-mediated cleavage of its proteoglycan substrate versican is critical for cardiac valve and limb development (McCulloch et al. 2009; Dupuis et al. 2011; Wang et al. 2012). Cleavage of Acan is crucial for appropriate tendon formation (McCulloch et al. 2009; Dupuis et al. 2011; Wang et al. 2012). This is the first study, to our knowledge, to investigate the role of ADAMTS5 in the MCC and demonstrate the requirement for ADAMTS5 to establish the normal fibrocartilage zonal architecture in the murine TMJ.

Materials and Methods

Adamts5-null *and Collagen X Reporter Mice*

The Medical University of South Carolina Institutional Animal Care and Use Committee (IACUC) approved this study. *Adamts5*$^{tm1DgenJ-}$ (Jackson Laboratories) mice on a C57Bl/6 background (McCulloch et al. 2009; Dupuis et al. 2011; Dupuis et al. 2013) and Col10a1-RFPchry (Col10-mCherry) reporter mice on a CD-1 background, provided by David W. Rowe, MD (Chen et al. 2012), were crossed to produce Col10-mCherry$^{+/+}$/*Adamts5*^{het} for breeding and littermates Col10-mCherry$^{+/-}$/*Adamts5*$^{+/+}$ and Col10-mCherry$^{+/-}$/*Adamts5*$^{-/-}$ for this study. Due to the mixed background (CD-1; C57Bl/6), the MCC phenotype in the Col10-mCherry$^{+/-}$/*Adamts5*$^{-/-}$ was compared to that of the Col10-mCherry$^{+/-}$/*Adamts5*$^{+/+}$ (n = 5/genotype) for mCherry expression using same gain-setting confocal images and quantified using Amira 6.3.0 (Visage Imaging) (Dupuis et al. 2011).

Tissue Collection, Histomorphometrics, and Immunohistochemistry

Adamts5$^{+/+}$ and *Adamts5*$^{-/-}$ mouse heads were bisected at 2 mo (n = 11 and n = 12, respectively). The left side was fixed in 4% paraformaldehyde, decalcified in 0.5 M ethylenediaminetetraacetic acid (EDTA) (pH 8.0) for 4 to 5 wk, and processed for histology and immunohistochemistry (IHC). Tissue was sectioned at 8 µm. Safranin O/Fast Green staining was used for histomorphometric analysis. Paraformaldehyde fixed tissues were stained for Acan (1:100 dilution; AB1031 Chemicon), type II collagen (1:100 dilution; ab34712, Abcam), and type X collagen (1:100 dilution; ab49945, Abcam). Nuclei were stained with propidium iodide (PI). The right condylar head was flash frozen in liquid nitrogen for protein/RNA analysis or fixed in 10% buffered formalin for 2 d. For cryosectioning, formalin-fixed condylar heads were processed through a sucrose gradient, mounted in optimal cutting temperature (OCT) embedding medium (Tissue-Tek) and sectioned at 20 µm. Nuclei were stained with PI and slides were mounted using DABCO (1,4-diazabicyclo[2.2.2]octane).

Gene Expression Analysis

Adamts5$^{+/+}$ and *Adamts5*$^{-/-}$ condylar heads were dissected from the mandible along the horizontal plane as indicated in Figure 1G. The hypertrophic layer was embedded with trabeculated bone, making it virtually impossible to ensure no trabeculated bone was present in the isolated condylar head tissue. However, the amount of contaminating trabeculated bone would be a small percentage of the total amount of tissue collected. In addition, a similar amount of trabeculated bone would be present in each *Adamts5*$^{+/+}$ and *Adamts5*$^{-/-}$ sample, thus normalizing any nonfibrocartilage contamination. Condylar heads were flash frozen in liquid nitrogen and stored at –80°C. Prior to RNA extraction, tissue was transferred to RNAlater-ICE Frozen Tissue Transition Solution (Ambion) for 16 h. Total RNA was isolated using RNeasy Plus Universal Mini Kit (Qiagen) following the manufacturer's protocol. Then, 100 ng of complementary DNA was synthesized using Quanta Biosciences qScript cDNA SuperMix (Thermo Fisher Scientific). Quantitative real-time polymerase chain reaction (qRT-PCR) was performed using TaqMan primer and probes (Applied Biosciences). Gene expression was assessed for aggrecan (*Acan*—Mm00545794_m1), collagen type II (*Col2A1*—Mm01309565), collagen type X (*Col10a1*—Mm00487041_m1), SRY-box containing gene 9 (*Sox9*—Mm00448840_m1), and parathyroid hormone–related protein (*Pthrp*—Mm00436057_m1) and normalized to β-actin (*Actb*—Mm02619580). The ΔΔCt method was used for gene expression analysis. For protein analysis, radio immunoprecipitation assay (RIPA) buffer extracts were Chondroitinase ABC treated, run on 3% to 8% reducing gradient gels, and probed with the Acan antibody (Appendix Fig. 5; AB1031 Chemicon) and β-actin antibody (ab8226, Abcam) for normalization.

Quantification and Statistical Analysis

Total MCC fibrocartilage, ECM, and cell volumes (24 µm depth; n = 11+) were quantified using Amira (Appendix Figs. 3 and 4). Digital images were acquired using the Leica TCS SP5 AOBS Confocal Microscope System, to quantify Acan (8 µm depth; n = 5/genotype for 3 technical replicates) and mCherry immunofluorescence (8 µm depth; n = 5/genotype). Confocal gain settings were set to a linear range using the most intense fluorescence emission. Pixel intensity of Acan and mCherry was measured by counting the total number of

positive pixels above a threshold value and normalizing to total cartilage volume. For fluorescence quantification, statistical significance was determined using Student's *t* test (2-tailed, type 2). The 1-sample *t* test was used for analysis of qRT-PCR data (Yuan et al. 2006). Statistical qRT-PCR data are presented as the mean ± standard error (SE). *Adamts5*$^{+/+}$ and *Adamts5*$^{-/-}$ Safranin O/Fast Green images were acquired with a Zeiss Axio.A1 Microscope. ZenBlue was used to measure cell lengths. For cell length data, values were grouped into 2-µm ranges and normalized to the total cell number per sample. The normalized outcomes were presented as mean percentage of cell lengths and SE (n = 11 *Adamts5*$^{+/+}$; n = 11 *Adamts5*$^{-/-}$). One-way analysis of variance was run to determine the effect of genotype on mean percentage of cell length ranges. Any P values <0.05 were considered statistically significant.

Modified Mankin Fibrocartilage Scoring

The Mankin scoring (van der Sluijs et al. 1992; Shen et al. 2015; Zhou et al. 2016) was modified to include the fibrocartilage chondrocyte parameter of axial row disruption. Evaluation of critical ECM components in murine MCC, including Acan, collagen II (Ricks et al. 2013), fibromodulin, and biglycan (Embree et al. 2010), replaced the variable Safranin O staining parameters. The modified murine Mankin scoring allows more precise characterization of the ECM changes that may be associated with murine TMJOA. Details of the modified murine Mankin fibrocartilage parameters are in the Appendix Methods.

Results

The Zonal Architecture of Mandibular Condylar Cartilage Is Altered in Adamts5$^{-/-}$ *Mice*

The impact of ADAMTS5 deficiency was evaluated on the MCC at postnatal day 7 (P7), at 1 mo and in young adult mice (2 mo; Fig. 1). At P7, in the *Adamts5*$^{-/-}$, there was an expansion in intercellular Safranin O staining where *Adamts5* was expressed (Fig. 1A–C). At 1 mo, the outer zone (Fig. 1E, F) was expanded in the *Adamts5*$^{-/-}$ MCC, a region where *Adamts5* was localized (Fig. 1D). In 2-mo *Adamts5*$^{+/+}$ mice, the MCC was divided into 4 zones (superficial, polymorphic, chondrocytic, and hypertrophic) (Fig. 1K). The zonal architecture of the *Adamts5*$^{-/-}$ MCC was dramatically altered (Fig. 1I, L). In the 2-mo *Adamts5*$^{+/+}$, there was intense red, Safranin O staining in the mature zones (Fig. 1H, K) that was reduced in the *Adamts5*$^{-/-}$ (Fig. 1I, L).

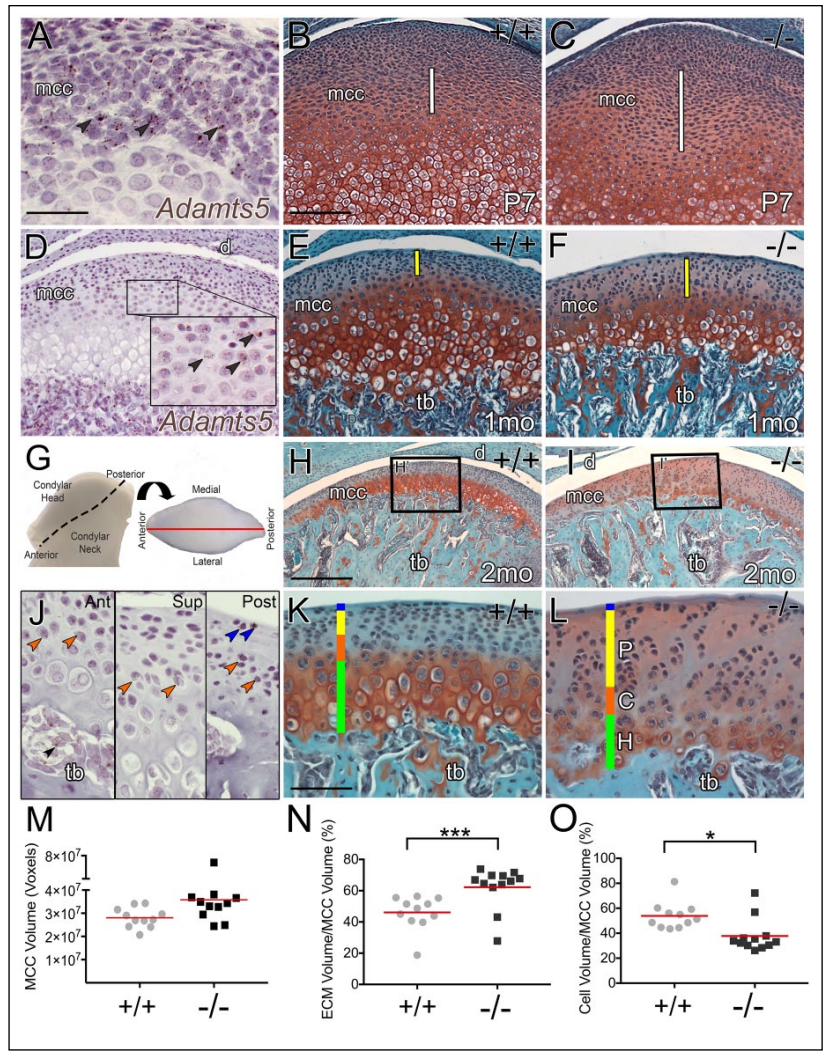

Figure 1. The zonal architecture of temporomandibular joint (TMJ) mandibular condylar cartilage (MCC) is disrupted in mice deficient in the extracellular matrix (ECM) protease, ADAMTS5. RNAscope in situ of *Adamts5* messenger RNA (**A**, **D**, **J**) in the developing MCC is shown with corresponding developing MCC Safranin O/Fast Green–stained sections of *Adamts5*$^{+/+}$ (+/+; **B**, **E**, **H**, **K**) and *Adamts5*$^{-/-}$ (–/–; **C**, **F**, **I**, **L**) at postnatal day 7 (P7; B, C), 1 mo (E, F), and 2 mo (H, I, K, L). White line (B, C) denotes expanded region in –/– MCC at P7. Yellow bar (E, F) denotes changes in polymorphic zone at 1 mo in –/– MCC. Fresh tissue image of 2-mo-old *Adamts5*$^{+/+}$ mandibular condyle; dashed line indicates the condylar head (**G**). Arrow denotes rotation for a superior view of the articulating surface (G). Black boxes H and I correspond to higher magnification in K and L, respectively. The graph in (**M**) represents total MCC fibrocartilage volume (P < 0.052) *Adamts5*$^{+/+}$ (n = 11) and *Adamts5*$^{-/-}$ (n = 12) using Amira. The graph in (**N**) shows the percent volume of extracellular matrix (ECM) in the MCC. The graph in (**O**) depicts the volume of cells in the MCC. Brown arrows (A, D) are an example of in situ *Adamts5*–positive cells in developing MCC; blue arrows, example of in situ *Adamts5*–positive cells in the superficial zone; orange arrows, in situ *Adamts5*–positive cells in the chondroblastic region; black arrow, in situ *Adamts5*–positive cells in trabeculated bone (tb). d, disc; mcc, mandibular condylar cartilage; blue bar, superficial zone; P, yellow bar = polymorphic zone; C, orange bar = chondrocytic zone; H, green bar = hypertrophic zone. Scale bars: A = 50 µm applies to D inset J to L. B = 100 µm applies to C, E, F. H = 200 µm applies to I. In M to O, red lines represent the mean. *$P \le 0.05$ and **$P \le 0.001$. This figure is available in color online.

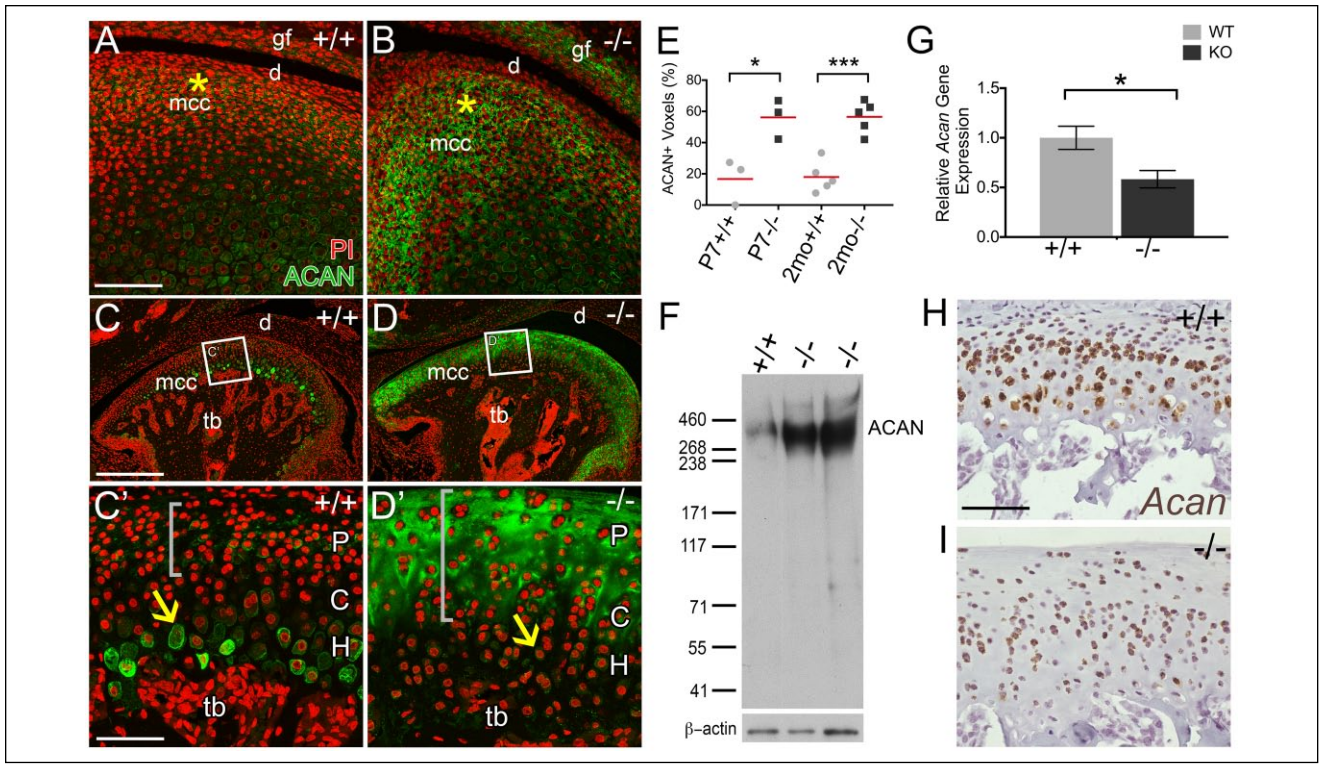

Figure 2. Aggrecan accumulates in *Adamts5*$^{-/-}$ mandibular condylar cartilage (MCC). Immunohistochemistry of aggrecan (ACAN; green) was performed on temporomandibular joint (TMJ) sections from 7-d-old (P7) murine MCC from *Adamts5*$^{+/+}$ (+/+; **A**, *n* = 3) and *Adamts5*$^{-/-}$ (–/–; **B**, *n* = 3) and 2-mo *Adamts5*$^{+/+}$ (+/+; **C**, **C′**, *n* = 5) and *Adamts5*$^{-/-}$ (–/–; **D**, **D′**, *n* = 5). Graph in **E** represents the percent ACAN in fibrocartilage within the interterritorial matrix of the polymorphic and chondrogenic zones of the superior region. Representative western blot of ACAN with molecular weight size markers denoted (**F**, *n* = 5); protein lysates were pretreated with Chondroitinase ABC. Quantitative real-time polymerase chain reaction of *Acan Adamts5*$^{+/+}$ (*n* = 5) and *Adamts5*$^{-/-}$ (*n* = 5) condylar heads (**G**) expressed as relative gene expression and represents $2^{-\Delta\Delta Ct}$ values. RNAscope of Acan messenger RNA expression in situ for 2-mo *Adamts5*$^{+/+}$ (**H**; brown) and *Adamts5*$^{-/-}$ (**I**; brown). C, chondrocytic layer; d, disc; H, hypertrophic layer; mcc, mandibular condylar cartilage; P, polymorphic layer; tb, trabeculated bone. Gray brackets indicate regions of pericellular matrix and interterritorial matrix ACAN localization of immature chondrocytes. Scale bar: A = 100 µm applies to B; C = 200 µm applies to D, C′ = 50 µm applies to D′. *$P \leq 0.05$ and ***$P \leq 0.0001$. This figure is available in color online.

The expanded interterritorial extracellular matrix of *Adamts5*$^{-/-}$ MCC (Fig. 1I, L) exhibited an increase in Safranin O staining. Several variables impacted the Safranin O staining in the MCC (Appendix Fig. 1). The MCC phenotype was characterized throughout the entire condylar depth (Appendix Fig. 2). Sections from the center of the condyle were used for subsequent analysis (Fig. 1G).

The volume of *Adamts5*$^{-/-}$ MCC fibrocartilage was quantified (Appendix Fig. 3) (Fig. 1M–O). The cell volume was quantified (Appendix Fig. 4) and was significantly reduced in the *Adamts5*$^{-/-}$ MCC (Fig. 1O). In addition, the *Adamts5*$^{-/-}$ MCC fibrocartilage had a statistically significant increase in ECM; this increased intercellular spacing was evident throughout all of the zones (Fig. 1K, L, N).

The ADAMTS5 Substrate Acan Accumulates in the Mandibular Condyle of Adamts5$^{-/-}$ *Mice*

To determine if accumulation of the ADAMTS5 substrate Acan contributes to the increase in ECM volume, IHC using an Acan antibody that recognizes an epitope within the central core of Acan (Appendix Fig. 5A) was performed on P7 and 2-mo *Adamts5*$^{+/+}$ and *Adamts5*$^{-/-}$ MCC (Fig. 2). The accumulation of Acan was evident at P7 in *Adamts5*$^{-/-}$ MCC (Fig. 2A, B, E) in the region where *Adamts5* was highly expressed (Fig. 1A). At 2 mo in the *Adamts5*$^{+/+}$ MCC, Acan was localized to the lacunae and pericellular matrix of hypertrophic chondrocytes with disperse staining in the ECM of the polymorphic zone (Fig. 2C, C′). The Acan IHC was significantly increased in the *Adamts5*$^{-/-}$ MCC, within the upper polymorphic and chondrocytic zones (Fig. 2D, D′, E) (Dupuis et al. 2011; Dupuis et al. 2013). Acan localization was increased throughout the entire condylar head, in *Adamts5*$^{-/-}$ MCC (Appendix Fig. 6). Western blots of *Adamts5*$^{+/+}$ and *Adamts5*$^{-/-}$ condylar heads also demonstrated a significant increase in the large intact Acan core protein in the *Adamts5*$^{-/-}$ MCC (Fig. 2F). qRT-PCR indicated that the increased Acan did not arise due to increased Acan messenger RNA (mRNA) (Fig. 2G). RNAscope in situ also showed a reduction in Acan mRNA in the *Adamts5*$^{-/-}$ MCC, indicating that Acan accumulation likely arose due to lack of turnover rather than increase in mRNA.

Fibrocartilage of the Mandibular Condyle in Adamts5$^{-/-}$ *Mice Has a Reduction in Hypertrophic Chondrocytes*

Cell volume was calculated and was significantly decreased in the *Adamts5*$^{-/-}$ (Fig. 3A). Cell counts indicated that the reduction of cell volume was not due to a change in cell number (Fig. 3B). However, the decrease in Safranin O staining in the hypertrophic zone of *Adamts5*$^{-/-}$ MCC indicated that the apparent loss of cellularity may be due to a reduction in large-sized hypertrophic chondrocytes. Lengths of all MCC cells were measured in 2-mo *Adamts5*$^{+/+}$ and *Adamts5*$^{-/-}$ (n = 11+, each genotype). The percentage of cells in each 2 µm size range was calculated and presented in a binning graph (Fig. 3C). The green square indicates the size range of mature hypertrophic chondrocytes; the mean percentage of *Adamts5*$^{-/-}$ cartilage cells with lengths between 16 and 24 µm was significantly less in the *Adamts5*$^{-/-}$ MCC (Fig. 3C–E). This reduction in large-sized cells was compensated by a higher percentage of cells in the 6- to 10-µm range (Fig. 3C). Since hypertrophic chondrocytes undergo apoptosis, a terminal deoxynucleotidyltransferase-mediated dUTP nick end labeling (TUNEL) assay was performed in P7, 1-mo, and 2-mo MCC to determine if the hypertrophic chondrocytes in the *Adamts5*$^{-/-}$ MCC were undergoing apoptosis at an increased rate (Appendix Fig. 7). However, the rate of apoptosis between the *Adamts5*$^{+/+}$ and *Adamts5*$^{-/-}$ MCC was unchanged. Collectively, these data suggest that a reduction in the number of large-sized hypertrophic cells contributes to disruption of the fibrocartilage zonal architecture in the *Adamts5*$^{-/-}$ MCC.

Chondrogenic Markers Were Reduced in the Mandibular Condylar Cartilage of Adamts5$^{-/-}$ *Mice*

The expression of chondrocytic maturation markers was evaluated within the *Adamts5*$^{-/-}$ MCC using 2-mo *Adamts5*$^{+/+}$ and *Adamts5*$^{-/-}$ condylar heads (Fig. 1G). SRY-box containing gene 9 (*Sox9*), collagen type II (*Col2a1*), and collagen type X (*Col10a1*) were significantly downregulated in the *Adamts5*$^{-/-}$ MCC (Fig. 4A). However, parathyroid hormone–related protein (*Pthrp*), a marker of the polymorphic zone, was not significantly altered between *Adamts5*$^{+/+}$ and *Adamts5*$^{-/-}$ MCC (Fig. 4A). IHC for type II collagen (Col2) and type X collagen (Col10) in *Adamts5*$^{+/+}$ and *Adamts5*$^{-/-}$ MCC (Fig. 4B–E) showed these mature cartilage proteins were reduced in the *Adamts5*$^{-/-}$ MCC. *Adamts5*$^{+/+}$ and *Adamts5*$^{-/-}$ mice were intercrossed with the Col10-mCherry reporter mice; hypertrophic chondrocytes are identified by their expression of the mCherry reporter driven by the Col10 promoter (Fig. 4F). The mCherry expression in ADAMTS5-deficient MCC was significantly diminished (Fig. 4G, H, I). These data indicate that markers associated with mature chondrocytes were reduced in the MCC of *Adamts5*$^{-/-}$ mice.

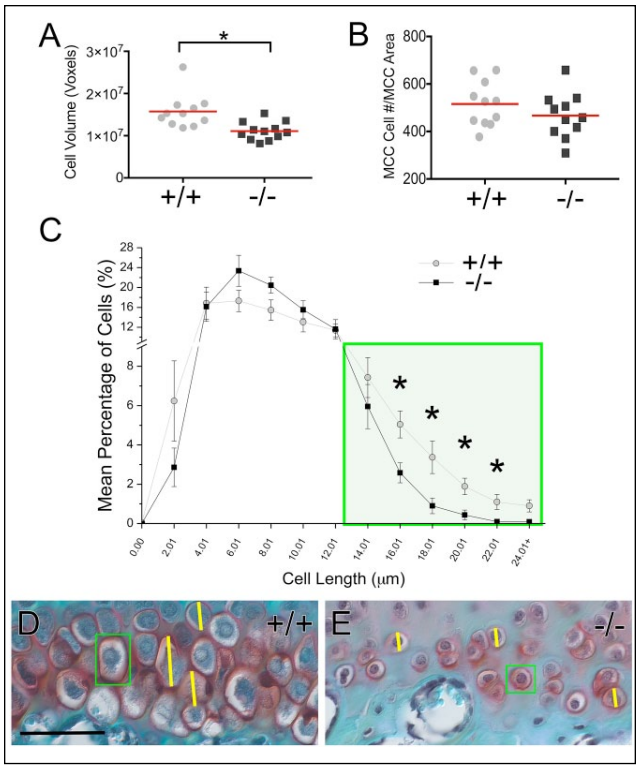

Figure 3. *Adamts5*$^{-/-}$ mandibular condylar cartilage (MCC) exhibits a reduction in large hypertrophic chondrocytes. Comparison of fibrocartilage cell volume of *Adamts5*$^{+/+}$ (+/+; n = 11) and *Adamts5*$^{-/-}$ (–/–; n = 12) was calculated for the MCC (**A**). Total number of cells in a 200× field of MCC was quantified (**B**). Lengths of all mandibular condylar cartilage cells were measured (ZenPro) for each murine MCC, grouped into 2-µm cell ranges using a binning graph. Y-axis indicates the percentage of cells in each size range (**C**). Green box denotes cell ranges that represent mature hypertrophic cells (i.e., length 16 to 24 µm) (C). **D** and **E** show Safranin O–stained images of the hypertrophic zone in 2-mo *Adamts5*$^{+/+}$ and *Adamts5*$^{-/-}$ condylar tissue. Green boxes (D and E) highlight hypertrophic fibrocartilage cells in 2-mo *Adamts5*$^{+/+}$ and *Adamts5*$^{-/-}$, respectively. Yellow lines denote diameter measurements. Scale bar: D = 50 µm applies to E. *$P \le 0.05$. This figure is available in color online.

Adamts5$^{-/-}$ *MCC Exhibit Higher Modified Mankin Scoring Compared to Wild Type*

To incorporate the extent to which the *Adamts5*$^{-/-}$ MCC phenotype exhibits changes associated with TMJOA, the *Adamts5*$^{+/+}$ and *Adamts5*$^{-/-}$ mice were aged to 6 mo (Fig. 5A, B) and evaluated based on modified Mankin scoring. Changes in chondrogenic arrangement indicative of early OA were increased in the *Adamts5*$^{-/-}$; hypertrophic cell atrophy (Fig. 5A, B, G), hypocellularity (Fig. 5H), cell clustering (Fig. 5B, I), and axial row disruption (Fig. 1A, B, F added based on this study) were observed. Since the Safranin O staining is variable and difficult to quantify in fibrocartilage, these Mankin parameters were replaced by examination of specific ECM components, including collagen II (Ricks et al. 2013) and proteoglycans Acan,

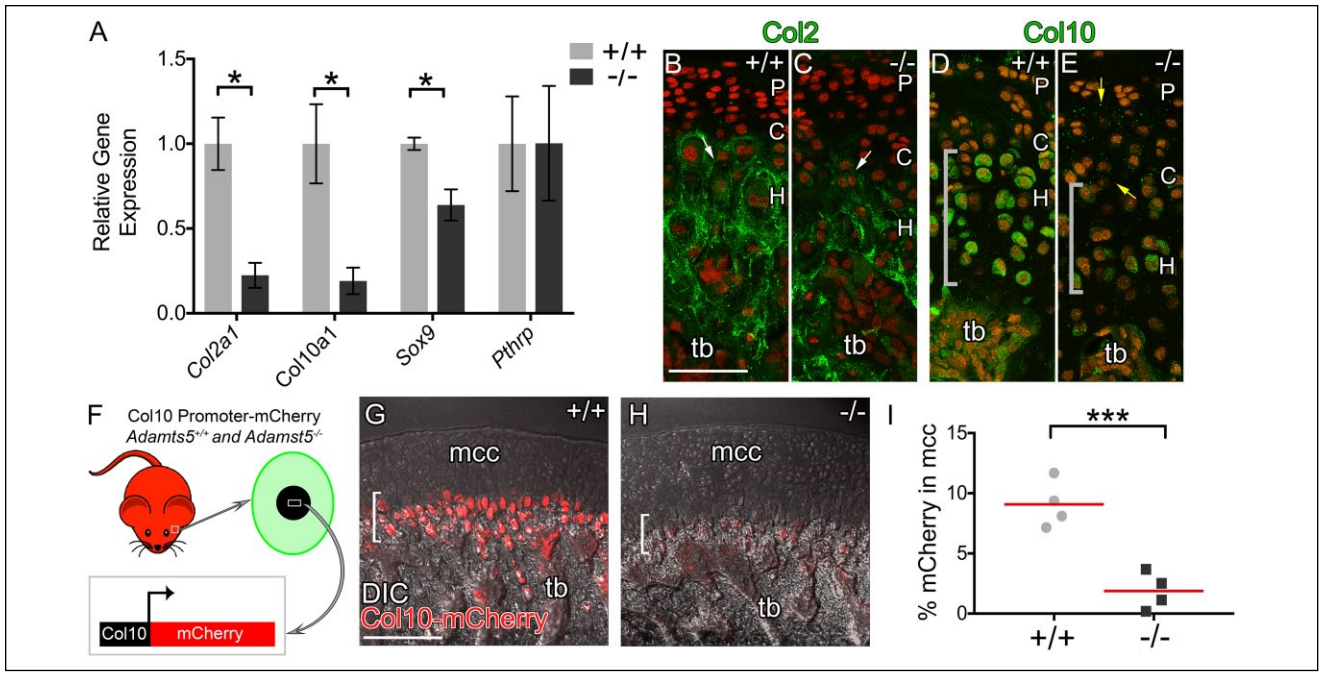

Figure 4. Expression of chondrogenic maturation markers in the mandibular condyle of *Adamts5*$^{-/-}$ mice is reduced. Quantitative real-time polymerase chain reaction: relative gene expression represents $2^{-\Delta\Delta Ct}$ values of *Col2a1, Col10a1, Sox9*, and *Pthrp* in *Adamts5*$^{+/+}$ (+/+, *n* = 5) and *Adamts5*$^{-/-}$ (–/–, *n* = 5) 2-mo condylar heads (**A**). Immunohistochemical staining for Col2 (green, B, C; white arrows) and Col10 (green, D, E; gray brackets) in *Adamts5*$^{+/+}$ (**B**, **D**) and *Adamts5*$^{-/-}$ (**C**, **E**) mandibular condyles. Interterritorial matrix Col10 staining denoted by yellow arrows (E). Propidium iodide (red, B–E) was used to stain nuclei. The ColX-mCherry reporter was used on the *Adamts5*$^{+/+}$ (+/+, *n* = 5) and *Adamts5*$^{-/-}$ (–/–, *n* = 5) mice and was active in hypertrophic chondrocytes (**F**, green cell) of the temporomandibular joint (F, white box). Col10-mCherry reporter mice at 2 mo; red mCherry expression in hypertrophic chondrocytes (brackets **G**, **H**). Percent mCherry expression was quantified in Amira and depicted in the graph in (**I**). C, chondrocytic layer; H, hypertrophic layer; P, polymorphic layer; tb, trabeculated bone. Scale bar: B, G = 100 µm applies to C–E.
*$P \leq 0.05$ and ***$P \leq 0.001$. This figure is available in color online.

biglycan, and fibromodulin (Embree et al. 2010). The higher modified Mankin fibrocartilage score (Fig. 5E) in the *Adamts5*$^{-/-}$ MCC and aging 6-mo *Adamts5*$^{+/+}$ and *Adamts5*$^{-/-}$ were derived from abnormal chondrogenic arrangements and changes in ECM composition but not alterations in cartilage structure, which are more indicative of advanced OA (Shen et al. 2015).

Discussion

These data indicate a critical and novel role for ADAMTS5 in the development of the MCC of the TMJ. In the absence of the ECM protease ADAMTS5, its substrate Acan accumulated, resulting in disrupted zonal organization. This correlated with a significant decrease in chondrocyte maturation markers and a marked decrease in mature hypertrophic chondrocytes, suggesting impaired chondrogenesis. It has been well established that Acan serves a protective role in cartilage contributing to its biomaterial properties (Kiani et al. 2002). However, our data demonstrate that Acan accumulation in the *Adamts5*$^{-/-}$ MCC impedes chondrogenic cell differentiation, indicating that this proteoglycan affects not only the biomaterial properties but also cell organization and differentiation. Furthermore, the increase in Acan also affected other critical cartilage components such as type II collagen, which is crucial for ECM structure and cartilage tensile strength to prevent cartilage OA (Mayne 1989; Poole et al. 2002). Acan accumulation resulted in a more dramatic increase to chondrogenic cell arrangements that have been associated with TMJOA. Of note, changes in the normal aging wild-type MCC were similar to the 2-mo ADAMTS5-deficient MCC. While depletion in Acan is associated with OA, these data indicate that an abnormal increase of Acan in the MCC may also be harmful to the TMJ. Active ADAMTS5-mediated regulation of Acan levels may be essential to normal development and homeostasis.

In the *Adamts5*$^{-/-}$ MCC, Acan accumulation in the polymorphic zone may impede signals necessary to promote chondrogenesis. *Adamts5*$^{-/-}$ chondrocyte differentiation appears to be affected in part due to a decrease in *Sox9* expression. SOX9 is the master regulator of chondrogenesis in cartilage and highly expressed by the chondroprogenitor cells where we observe Acan accumulation (Akiyama et al. 2002; Ikegami et al. 2011). The excess Acan likely affects chondrogenesis because the ECM architecture functions as a scaffold that stores growth factors and ligands; therefore, ECM turnover by proteases such as ADAMTS5 may be necessary for the release of growth factors required to promote chondrogenic maturation during MCC fibrocartilage development (Gao et al. 2014).

Active Acan turnover produces small aggrecan fragments via ADAMTSs and MMP cleavage, which have associations with both cartilage homeostasis and disease. While Acan processing has not been studied in the context of TMJ fibrocartilage,

ex vivo articular chondrocyte culture studies demonstrate that G1 domain fragments, ITEGE373 and DIPEN374, are internalized through CD44-hyluranon interactions (Embry Flory et al. 2006; Ariyoshi et al. 2010). Yet, it is unclear how Acan fragment internalization affects chondrocyte identity and behavior. Acan turnover is increased in hyaline cartilage OA disease. Serum, synovial fluid, and tissue samples obtained from patients with knee OA contained greater amounts of Acan fragments ITEGE373 and DIPEN374 compared to healthy patient samples (Lark et al. 1997; Struglics et al. 2006; Kalai et al. 2012). This increased release of fragments presumably could lead to an increase in fragment internalization. OA tissue is also characterized by greater chondrocyte hypertrophy, resulting initially in hypercellularity with a transition to hypocellularity in late-stage disease (van der Kraan and van den Berg 2012). Our data demonstrate that the *Adamts5*$^{-/-}$ MCCs have smaller hypertrophic cells with a decrease in expression of hypertrophic markers *Col10a1* and type X collagen that correlated with Acan accumulation. However, in aged wild-type MCC, there was a significant decrease in hypertrophic chondrogenic size, indicating that the reduction of larger hypertrophic cells in the 2-mo *Adamts5*$^{-/-}$ MCC may be indicative of premature aging. Future studies are required to determine if Acan cleavage and subsequent fragment internalization are critical mechanisms for chondrocyte hypertrophy in the MCC.

This investigation has demonstrated the requirement for ADAMTS5 in the MCC to generate and to maintain zonal architecture; furthermore, the loss of ADAMTS5 resulted in a dramatic increase in its substrate Acan. The MCC of young ADAMTS5-deficient mice exhibited changes in cell organization associated with early OA disease. Since this protease is a therapeutic target for the treatment of OA progression, understanding its physiological role in the TMJ fibrocartilage will be important to determine any potential off-target effects of this treatment strategy. Moreover, effective interventions to prevent OA of hyaline cartilage, including reduction of ADAMTS5, may not be applicable for TMJ fibrocartilage.

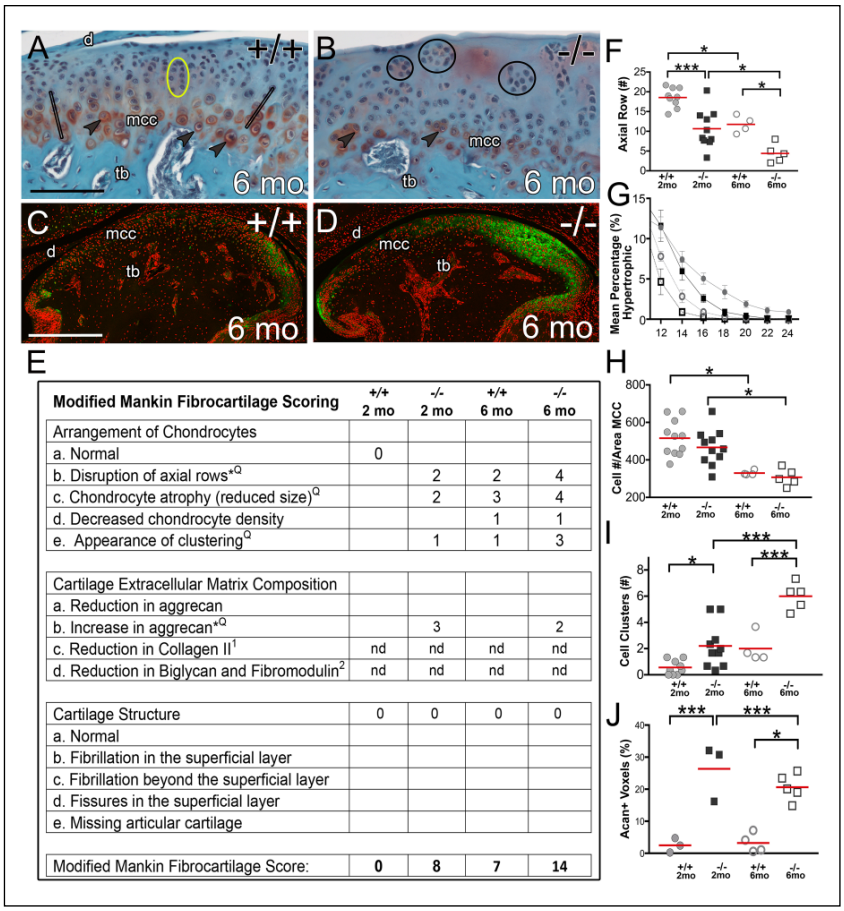

E

Modified Mankin Fibrocartilage Scoring	+/+ 2 mo	-/- 2 mo	+/+ 6 mo	-/- 6 mo
Arrangement of Chondrocytes				
a. Normal	0			
b. Disruption of axial rows*Q		2	2	4
c. Chondrocyte atrophy (reduced size)Q		2	3	4
d. Decreased chondrocyte density			1	1
e. Appearance of clustering Q		1	1	3
Cartilage Extracellular Matrix Composition				
a. Reduction in aggrecan				
b. Increase in aggrecan*Q		3		2
c. Reduction in Collagen II[1]	nd	nd	nd	nd
d. Reduction in Biglycan and Fibromodulin[2]	nd	nd	nd	nd
Cartilage Structure	0	0	0	0
a. Normal				
b. Fibrillation in the superficial layer				
c. Fibrillation beyond the superficial layer				
d. Fissures in the superficial layer				
e. Missing articular cartilage				
Modified Mankin Fibrocartilage Score:	0	8	7	14

Figure 5. Modified Mankin scoring indicates aging *Adamts5*$^{-/-}$ mandibular condylar cartilage exhibits a higher score of OA progression than wild-type mice. Safranin O–stained parasagittal sections of 6-mo-old *Adamts5*$^{+/+}$ (n = 4) (**A**) and *Adamts5*$^{-/-}$ (n = 5) (**B**) mandibular condylar cartilage. Acan immunolocalization (green) for *Adamts5*$^{+/+}$ (**C**) and *Adamts5*$^{-/-}$ (**D**) is shown. Modified Mankin fibrocartilage scoring table (**E**) for 2-mo *Adamts5*$^{+/+}$ (n = 11) and *Adamts5*$^{-/-}$ (n = 11) as well as 6-mo *Adamts5*$^{+/+}$ (n = 4) and *Adamts5*$^{-/-}$ (n = 5). Quantification of chondrocyte arrangements and Acan accumulation are shown in **F** to **J**. Q in the Mankin table (E) indicates additional quantification provided and * in table (E) indicates added criteria based on this study. Open black bars (A) denote axial rows, quantified in F; arrowheads indicate hypertrophic chondrocytes, indicative of atrophy and quantified in G; yellow eclipse highlights normal isogenous groups (A); circle outlines (B) indicate hypercellular clusters graphed in I. Graph depicting Acan percent positive voxels, including anterior, superior, and posterior regions, is shown in J. Graph symbols: solid circles, 2-mo *Adamts5*$^{+/+}$; solid squares, 2-mo *Adamts5*$^{-/-}$; open circles, 6-mo *Adamts5*$^{+/+}$; open squares, 6-mo *Adamts5*$^{-/-}$. d, disc; mcc, mandibular condylar cartilage; nd, not determined. Scale bar: A = 100 µm applies to B, C = 250 µm and applies to D. *$P \le 0.05$ and ***$P \le 0.001$. This figure is available in color online.

Author Contributions

C.B. Kern, contributed to conception, design, data analysis, and interpretation, drafted and critically revised the manuscript; A.W. Rogers, contributed to conception, design, data acquisition, analysis, and interpretation, drafted and critically revised the manuscript; S.E. Cisewski, contributed to data acquisition and analysis, critically revised the manuscript. All authors gave final approval and agree to be accountable for all aspects of the work.

Acknowledgments

This work was supported by National Institutes of Health grants RO1-HL-121382 (CBK), T32-DE-017551, P30-GM-103342, and P30-NIGMS-103331. We would like to give special thanks to MUSC's Center for Oral Health Research Laboratory and the Josh Spruill Imaging facilities for use of their equipment. We want to

recognize D. Lake Billings for his histology work. In addition, we thank Abigail Kelly and Dr. Jim Cray for statistical consultation. The authors declare no potential conflicts of interest with respect to the authorship and/or publication of this article.

References

Akiyama H, Chaboissier MC, Martin JF, Schedl A, de Crombrugghe B. 2002. The transcription factor Sox9 has essential roles in successive steps of the chondrocyte differentiation pathway and is required for expression of Sox5 and Sox6. Genes Dev. 16(21):2813–2828.

Ariyoshi W, Knudson CB, Luo N, Fosang AJ, Knudson W. 2010. Internalization of aggrecan G1 domain neoepitope ITEGE in chondrocytes requires CD44. J Biol Chem. 285(46):36216–36224.

Benjamin M, Ralphs JR. 2004. Biology of fibrocartilage cells. Int Rev Cytol. 233:1–45.

Chen J, Utreja A, Kalajzic Z, Sobue T, Rowe D, Wadhwa S. 2012. Isolation and characterization of murine mandibular condylar cartilage cell populations. Cells Tissues Organs. 195(3):232–243.

Chu WC, Zhang S, Sng TJ, Ong YJ, Tan WL, Ang VY, Foldager CB, Toh WS. 2017. Distribution of pericellular matrix molecules in the temporomandibular joint and their chondroprotective effects against inflammation. Int J Oral Sci. 9(1):43–52.

Dupuis LE, McCulloch DR, McGarity JD, Bahan A, Wessels A, Weber D, Diminich AM, Nelson CM, Apte SS, Kern CB. 2011. Altered versican cleavage in ADAMTS5 deficient mice: a novel etiology of myxomatous valve disease. Dev Biol. 357(1):152–164.

Dupuis LE, Osinska H, Weinstein MB, Hinton RB, Kern CB. 2013. Insufficient versican cleavage and Smad2 phosphorylation results in bicuspid aortic and pulmonary valves. J Mol Cell Cardiol. 60:50–59.

Embree MC, Kilts TM, Ono M, Inkson CA, Syed-Picard F, Karsdal MA, Oldberg A, Bi Y, Young MF. 2010. Biglycan and fibromodulin have essential roles in regulating chondrogenesis and extracellular matrix turnover in temporomandibular joint osteoarthritis. Am J Pathol. 176(2):812–826.

Embry Flory JJ, Fosang AJ, Knudson W. 2006. The accumulation of intracellular ITEGE and DIPEN neoepitopes in bovine articular chondrocytes is mediated by CD44 internalization of hyaluronan. Arthritis Rheum. 54(2):443–454.

Fosang AJ, Last K, Stanton H, Golub SB, Little CB, Brown L, Jackson DC. 2010. Neoepitope antibodies against MMP-cleaved and aggrecanase-cleaved aggrecan. In: Clark IM, editor. Matrix metalloproteinase protocols. Totowa (NJ): Humana Press. p. 305–340.

Gao Y, Liu S, Huang J, Guo W, Chen J, Zhang L, Zhao B, Peng J, Wang A, Wang Y, et al. 2014. The ECM-cell interaction of cartilage extracellular matrix on chondrocytes. Biomed Res Int. 2014:648459.

Glasson SS, Askew R, Sheppard B, Carito B, Blanchet T, Ma HL, Flannery CR, Peluso D, Kanki K, Yang Z, et al. 2005. Deletion of active ADAMTS5 prevents cartilage degradation in a murine model of osteoarthritis. Nature. 434(7033):644–648.

Ikegami D, Akiyama H, Suzuki A, Nakamura T, Nakano T, Yoshikawa H, Tsumaki N. 2011. Sox9 sustains chondrocyte survival and hypertrophy in part through Pik3ca-Akt pathways. Development (Cambridge, England). 138(8):1507–1519.

Kalai E, Bahlous A, Charni N, Bouzid K, Sahli H, Laadhar L, Chelly M, Rajhi H, Zouari B, Makni S, et al. 2012. Association of serum levels of aggrecan ARGS, NITEGE fragments and radiologic knee osteoarthritis in Tunisian patients. Joint Bone Spine. 79(6):610–615.

Kelwick R, Desanlis I, Wheeler GN, Edwards DR. 2015. The ADAMTS (a disintegrin and metalloproteinase with thrombospondin motifs) family. Genome Biol. 16:113.

Kiani C, Chen L, Wu YJ, Yee AJ, Yang BB. 2002. Structure and function of aggrecan. Cell Res. 12(1):19–32.

Kintakas C, McCulloch DR. 2011. Emerging roles for ADAMTS5 during development and disease. Matrix Biol. 30(5–6):311–317.

Knudson CB. 1993. Hyaluronan receptor-directed assembly of chondrocyte pericellular matrix. J Cell Biol. 120(3):825–834.

Lark MW, Bayne EK, Flanagan J, Harper CF, Hoerrner LA, Hutchinson NI, Singer II, Donatelli SA, Weidner JR, Williams HR, et al. 1997. Aggrecan degradation in human cartilage: evidence for both matrix metalloproteinase and aggrecanase activity in normal, osteoarthritic, and rheumatoid joints. J Clin Invest. 100(1):93–106.

Li W, Wu M, Jiang S, Ding W, Luo Q, Shi J. 2014. Expression of ADAMTS-5 and TIMP-3 in the condylar cartilage of rats induced by experimentally created osteoarthritis. Arch Oral Biol. 59(5):524–529.

Mayne R. 1989. Cartilage collagens: what is their function, and are they involved in articular disease? Arthritis Rheum. 32(3):241–246.

McCulloch DR, Nelson CM, Dixon LJ, Silver DL, Wylie JD, Lindner V, Sasaki T, Cooley MA, Argraves WS, Apte SS. 2009. ADAMTS metalloproteases generate active versican fragments that regulate interdigital web regression. Dev Cell. 17(5):687–698.

Plaas A, Osborn B, Yoshihara Y, Bai Y, Bloom T, Nelson F, Mikecz K, Sandy JD. 2007. Aggrecanolysis in human osteoarthritis: confocal localization and biochemical characterization of ADAMTS5-hyaluronan complexes in articular cartilages. Osteoarthritis Cartilage. 15(7):719–734.

Poole AR, Kobayashi M, Yasuda T, Laverty S, Mwale F, Kojima T, Sakai T, Wahl C, El-Maadawy S, Webb G, et al. 2002. Type II collagen degradation and its regulation in articular cartilage in osteoarthritis. Ann Rheum Dis. 61(Suppl 2):II78–II81.

Pratta MA, Yao W, Decicco C, Tortorella MD, Liu RQ, Copeland RA, Magolda R, Newton RC, Trzaskos JM, Arner EC. 2003. Aggrecan protects cartilage collagen from proteolytic cleavage. J Biol Chem. 278(46):45539–45545.

Rabie AB, Xiong H, Hägg U. 2004. Forward mandibular positioning enhances condylar adaptation in adult rats. Eur J Orthod. 26(4):353–358.

Ricks ML, Farrell JT, Falk DJ, Holt DW, Rees M, Carr J, Williams T, Nichols BA, Bridgewater LC, Reynolds PR, et al. 2013. Osteoarthritis in temporomandibular joint of Col2a1 mutant mice. Arch Oral Biol. 58(9):1092–1099.

Shen P, Jiao Z, Zheng JS, Xu WF, Zhang SY, Qin A, Yang C. 2015. Injecting vascular endothelial growth factor into the temporomandibular joint induces osteoarthritis in mice. Sci Rep. 5:16244.

Sobue T, Yeh WC, Chhibber A, Utreja A, Diaz-Doran V, Adams D, Kalajzic Z, Chen J, Wadhwa S. 2011. Murine TMJ loading causes increased proliferation and chondrocyte maturation. J Dent Res. 90(4):512–516.

Stanton H, Rogerson FM, East CJ, Golub SB, Lawlor KE, Meeker CT, Little CB, Last K, Farmer PJ, Campbell IK, et al. 2005. ADAMTS5 is the major aggrecanase in mouse cartilage in vivo and in vitro. Nature. 434(7033):648–652.

Struglics A, Larsson S, Pratta MA, Kumar S, Lark MW, Lohmander LS. 2006. Human osteoarthritis synovial fluid and joint cartilage contain both aggrecanase- and matrix metalloproteinase–generated aggrecan fragments. Osteoarthritis Cartilage. 14(2):101–113.

van der Kraan PM, van den Berg WB. 2012. Chondrocyte hypertrophy and osteoarthritis: role in initiation and progression of cartilage degeneration? Osteoarthritis Cartilage. 20(3):223–232.

van der Sluijs JA, Geesink RG, van der Linden AJ, Bulstra SK, Kuyer R, Drukker J. 1992. The reliability of the Mankin score for osteoarthritis. J Orthop Res. 10(1):58–61.

Wang VM, Bell RM, Thakore R, Eyre DR, Galante JO, Li J, Sandy JD, Plaas A. 2012. Murine tendon function is adversely affected by aggrecan accumulation due to the knockout of ADAMTS5. J Orthop Res. 30(4):620–626.

Wilusz RE, Sanchez-Adams J, Guilak F. 2014. The structure and function of the pericellular matrix of articular cartilage. Matrix Biol. 39:25–32.

Yuan JS, Reed A, Chen F, Stewart CN, Jr. 2006. Statistical analysis of real-time PCR data. BMC Bioinformatics. 7:85.

Zhou S, Xie Y, Li W, Huang J, Wang Z, Tang J, Xu W, Sun X, Tan Q, Huang S, et al. 2016. Conditional deletion of Fgfr3 in chondrocytes leads to osteoarthritis-like defects in temporomandibular joint of adult mice. Sci Rep. 6:24039.